Applied Thermal Engineering 100 (2016) 256–266

Contents lists available at ScienceDirect

Applied Thermal Engineering

journal homepage: www.elsevier.com/locate/apthermeng

Research Paper

Numerical simulation of a rising bubble with phase change

Seungwon Shin [a,*], Beomjoon Choi [b]

[a] Department of Mechanical and System Design Engineering, Hongik University, Sangsu-dong, 72-1, Mapo-gu, Seoul 121-791, Republic of Korea
[b] Department of Mechanical Engineering, Hongik University, Seoul 121-791, Republic of Korea

HIGHLIGHTS

- Efficient and stable way of sharp energy method for two-phase flow with phase change is proposed.
- General implementation process for proposing sharp energy method was described.
- Several phase change formulations are compared for their accuracy.
- Benchmarking tests were performed to show the accuracy of the proposed algorithm.

ARTICLE INFO

Article history:
Received 24 November 2015
Accepted 7 February 2016
Available online 13 February 2016

Keywords:
Direct numerical simulation
Multiphase flow
Phase change process
Sharp energy method
Interface dynamics

ABSTRACT

In this paper, efficient and stable way of sharp energy method for two-phase flow with phase change is proposed. General discretization procedure for the implementation of the proposed method is also described. Compared to existing sharp energy formulations, the proposed method does not require any cut-off value for solution stability. Several different formulations of the mass source term at the phase changing interface were compared for their accuracy. Theoretical solution of a bubble growth in a stagnant liquid with zero gravity was used to identify the proper choice of the necessary formulation. After fixing the right formulation, probing distance for the temperature gradients to compute mass transfer rate at the interface was tested for optimal grid convergence. Probing distance of 0.75 times the grid size with first order approximation was found to be generally optimal for the best grid convergence within considered working resolution. A bubble rise with phase change was simulated and compared with experimental data. The bubble growth rate from the simulation was well compared with experiment.

1. Introduction

Phase change process especially related to gas and liquid is a very important physical phenomenon that determines the fundamental behavior of various thermal engineering equipment. Due to difficulties with accurate measurement of local data during phase changing process, overall characteristics such as heat transfer rate are usually measured for analysis. Detailed temperature, as well as velocity field associated with local phase change behavior, is hard to obtain. To understand underlying physical behavior more clearly, detailed velocity and temperature distribution must be acquired and analyzed. On this respect, a numerical tool can be ideal in providing necessary temperature and velocity profile for the intended analysis.

Numerical simulation of two-phase flow has become very popular, and several techniques such as Volume of Fluid [1], Level Set [2], and Front Tracking [3] method are being widely used throughout various engineering platforms. However, most formulations are focused on the hydraulic part of the interface dynamics. More accurate tracking capability regarding precise positioning along with volume conservation is usually the main issue. In addition to proper capturing of moving interface, phase change process bears several difficulties during numerical modeling. For instance, phase change formulation should account correct mass generation from the interface. Most of the interface tracking formulation with phase change has been focused on boiling problem especially for film or nucleate boiling. Juric and Tryggvason [4] applied Front Tracking method to simulate film boiling problem. Detailed interface temperature condition was modeled and two-dimensional film boiling was analyzed. Son et al. [5] used Level Set method to simulate single nucleate boiling on horizontal surface in two-dimensional axi-symmetrical geometry. Microlayer model was developed to account correct phase interface boundary condition at the wall contact. Numerical results of interface evolution were compared well with experimental measurement. Esmaeeli and Tryggvason [6] improve the procedure proposed by Juric and Tryggvason [4] by eliminating the iteration process while applying interface temperature boundary condition. The method was applied to three-dimensional film boiling problem. Luo et al. [7] introduced subcell concept to increase the accuracy of interface mass transfer for Level Set method. The method was

* Corresponding author. Tel.: +82 2 320 3038; fax: +82 2 322 7003.
E-mail address: sshin@hongik.ac.kr (S. Shin).

http://dx.doi.org/10.1016/j.applthermaleng.2016.02.025
1359-4311/

expanded to three-dimensional simulation of single nucleate boiling. To increase the applicability of the solution, complex shapes of solid boundary are embedded with phase change formulation [8–10]. Dynamic process associated with bubble growth and detachment during nucleate boiling drew quite attentions from many researchers, and there are plenty of other related works regarding numerical simulation of boiling phenomenon [11,12].

Most two-phase flow simulations utilize continuous surface tension formulation to solve each phase equation simultaneously [4–12]. Interfacial source term will be embedded in governing equation by delta function term, which generates necessary forces or mass transfer just near the interface. Recently, ghost type method has become very popular for the hydraulic part of two-phase simulation [13–16]. It basically solves two separate momentum equations in each phase. Pressure jump condition across the interface will be applied very sharply. With proper modulation of the pressure jump, parasitic current can be regulated considerably. Fedkiw et al. [13] applied ghost fluid method to prevent smearing of the distance function during interface evolution by Level Set method. The sharpness of the density field can be maintained without oscillation near the interface by adopting band of ghost cells near the interface. Various improvements and modifications were accompanied in the frame work of specific two-phase simulation techniques [14–16]. Lately, energy equation is also being treated with sharp interface method [11,17–19].

For the energy equation, sharp interface method becomes more attractive compared to the momentum equation. In case of delta-function type methods to prescribe phase boundary condition, several iterations are necessary to satisfy specific interface condition [4], i.e. Dirichlet condition of fixed saturation temperature. Without proper iteration, there can be temperature overshoot near the phase interface. With sharp method, fixed temperature can be precisely enforced at the phase interface without temperature overshoot. Several procedures for efficient implementation of the ghost type method have been devised mostly for Level Set and Volume of Fluid methods. Yang and Udaykumar [17] developed sharp interface Cartesian grid method especially for pure material solidification using Level Set method. General procedure for the implementation of the proposed method was fully described. Gibou et al. [18] also applied sharp interface technique for energy equation. The interface motion was captured by Level Set function and the proposed algorithm was applied to analyze the interface motion of film boiling. Sato and Niceno [19] developed a very detailed procedure of sharp interface method for both momentum and energy equation. Volume of Fluid method was utilized to capture the interface location. Mass transfer was computed directly from the phase changing interface and distributed sharply to specific phase for correct velocity jump condition. The proposed model was compared with exact solution for single vapor bubble growth in superheated liquid with zero gravity. Simulation results showed excellent agreement with theoretical solution for several different parameters. Rising vapor bubble in superheated liquid with phase change was also compared with experimental measurement and matched very well. The developed method was applied to nucleate boiling problem with microlayer evaporation model at the contact point.

For most formulations of the sharp energy method, temperature at ghost points is usually extrapolated using values at the phase interface and neighboring inner grid points [17–19]. When the interface becomes very close to the inner grid points, sharp method could generate excessive gradient causing solution instability. To prevent sudden change of the gradient, the distance to the nearest inner grid point from the interface could be filtered with specific minimum value [17]. Since the gradient fluctuation due to proximity of the interface to the interpolating grid points is localized phenomenon, filtering usually does not affect overall accuracy very much. However, selecting appropriate filtering value can be arbitrary depending on problems at hand, and sometimes minor tweaks of the simulation conditions are necessary for stable simulation. Shin et al. [20] formulated an efficient way of utilizing regular grid structure that minimizes proximity of the interface to the grid points with Level Contour Reconstruction Method (LCRM) [21]. LCRM combines Front Tracking and Level Set methods to take advantages associated with each method. In this paper, more efficient procedure of the numerical formulation will be provided for general three-dimensional simulation. We will also concentrate on evaluating the correct formulation for phase changing terms in Front Tracking-based method. Several different formulations for phase changing source term will be analyzed and compared with benchmarking solution. Some procedural improvements from the previous version will also be described.

2. Numerical formulation

2.1. Interface tracking method

Front tracking type method utilizes separate interface elements to track evolving interface on top of regular Cartesian grid for velocity and pressure. To track or locate freely moving interface, additional Lagrangian elements can be very effective for precise positioning of the phase boundary. Correct boundary condition for momentum and energy equation will be accounted by implementing proper source term directly at the interface. However, phase tracking based on Front Tracking becomes a non-trivial problem, especially for three-dimensional simulation to maintain uniformity of the interface elements. On the other hand, front capturing type method implicitly locates phase boundary by solving additional Eulerian advection equation of the scalar field for phase indicator such as local volume (Volume of Fluid) or distance function to the interface (Level Set). Since additional scalar field uses exactly the same grid structure as velocity and pressure, formulation becomes relatively easy and straightforward. Some drawbacks such as continuity (VOF) and diffusivity (LS) of the interface were noticed and various remedies have been reported to overcome those difficulties.

In this paper, we will utilize Level Contour Reconstruction Method (LCRM) to track the moving interface. LCRM hybridizes Front Tracking and Level Set methods to combine the advantages of each method. Basic concept of the LCRM is depicted in Fig. 1. LCRM basically tracks additional Lagrangian interface similar to Front Tracking and it also generates distance function directly from the interface

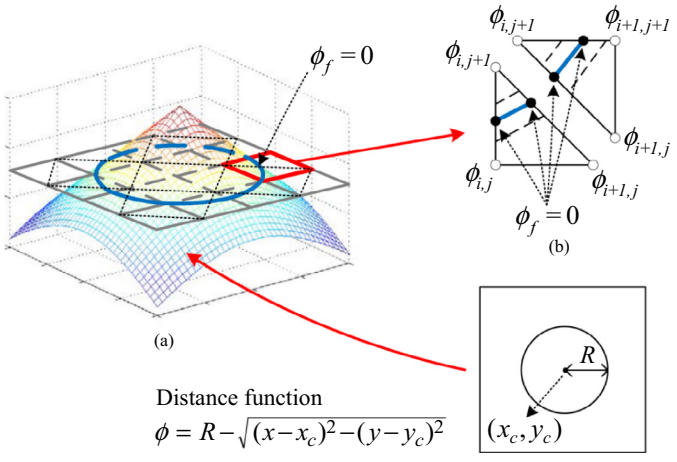

Fig. 1. Brief description of the Level Contour Reconstruction Method. (a) Distance function field (ϕ) with contour lines at $\phi = 0$; (b) domain decomposition for tetra-marching reconstruction.

location. Interface elements are periodically reconstructed by drawing contour line along specific value of the distance function, which related to Level Set characteristics (see Fig. 1(a)). So the regenerated interface elements would maintain a certain distance from each other, preventing excessive coagulation or dispersion. Underlying grid cells for primary variables such as velocity, pressure, and temperature were divided into triangular cells for tetra-marching reconstruction (Fig. 1(b)). A triangular (or tetrahedral for 3D) cell will guarantee single contour line (or surface) in each reconstruction cell. Several other upgrades have been done so far. More precise allocation of the interface location can be obtained using high order reconstruction technique [22]. Curvature computation was modified also by mixing Front Tracking and Front Capturing concepts [23]. Hybrid surface tension force can keep spurious current to minimal level even with microscale computation. Lately, three-dimensional code has been parallelized for massively distributed computation. Hydrodynamic performance of the numerical technique has been well benchmarked through various studies [20–24].

2.2. Sharp energy method

For the problem with moving interface, applying correct boundary condition is the most crucial part in designing proper numerical scheme. Lately, ghost type method has become very popular since it can apply specific boundary condition directly onto the phase interface. Pressure jump condition across the interface can be prescribed at ghost points to solve separate momentum equations simultaneously for both liquid and gas phases. However, the required boundary condition for the pressure is Neumann condition, so the general formulation for three-dimensional geometry is usually non-trivial. Compared to the momentum equation, energy equation can be more effectively solved by sharp formulation since the phase boundary condition is mostly fixed value, i.e. Dirichlet condition. Several formulations of ghost type method regarding energy diffusion term have been proposed [17,19]. The ghost point values for each phase are extrapolated using the phase boundary condition and the values from inner grid points within the intended computational domain. This formulation has critical drawback when the interface becomes very close to the interpolating grid points. If the distance between the interface and the grid node becomes small, the gradient using those two points gets very unstable, showing singular behavior. So the gradients are usually filtered with minimal acceptable value to prevent solution break down. Since such proximity of the interface element to the grid point is limited to a small area, overall error could be in acceptable range [17]. Even with minor effect from local instability, stable solution cannot be guaranteed, so proper choice of the filtering value and simulation time step could be an important issue.

To alleviate such instability, Shin et al. [20] proposed a slight different approach to approximate temperature gradients in each phase for the sharp energy formulation. Here, we will pay more attention to efficient implementation of the algorithm by developing a general form of the discretization operator especially for the diffusion term. To compute accurate interface position, we utilized 2nd order ENO scheme for convection term in both momentum and energy equations with non-conservative form. We found out that sharp energy formulation for convection term does not increase the accuracy of the solution, so conventional form of the 2nd order ENO scheme was directly applied to both phases.

Before the generalization of the diffusion operator, we will briefly summarize the proposed sharp energy method. The concept and algorithm are basically the same as proposed in a previous study [20]. For simplicity, two-dimensional schematic for the general concept is shown in Fig. 2. Application to three-dimensional geometry is very straightforward by adding the additional z directional component. Diffusion term of the energy equation can be cast into the following form of sharp energy formulation:

$$\frac{1}{\rho c}\nabla\cdot k(\nabla T)=\frac{1}{\rho c}\left[\frac{\partial}{\partial x}\left(k\frac{\partial T}{\partial x}\right)+\frac{\partial}{\partial y}\left(k\frac{\partial T}{\partial y}\right)\right]=\alpha\left[\frac{\partial^2 T}{\partial x^2}+\frac{\partial^2 T}{\partial y^2}\right]$$
$$=\alpha_{i,j}\left[\frac{T_{+x}+T_{-x}-2T_{i,j}}{(\Delta x)^2}+\frac{T_{+y}+T_{-y}-2T_{i,j}}{(\Delta y)^2}\right] \quad (1)$$

Material properties become constant at each phase and its value will be assigned using distance function (ϕ) computed directly from the interface location [24]. If the vapor is in positive distance function field ($\phi_{i,j}>0$) and liquid in the other ($\phi_{i,j}<0$), then property field for the thermal diffusivity is:

$$\alpha_{i,j}=\alpha_G|\max(\phi_{i,j},0)|+\alpha_L|\min(\phi_{i,j},0)| \quad (2)$$

where subscripts L and G represent liquid and vapor phases, respectively. To compute diffusion term descried in Eq. (1), $T_{\pm x}$, $T_{\pm y}$ terms should be properly computed using sharp energy method.

At first, two different phases are separated and solved independently as in Fig. 2(a). Each phase uses its own ghost values to accommodate the correct phase boundary condition, i.e. saturation temperature at the interface. Ghost values are extrapolated to satisfy correct phase boundary condition. For example, the ghost value in x direction for the liquid side (see point T_{-x} in Fig. 2(b)) can be computed using the phase interface condition and the value interpolated from the grid nodes (point T_{intp_x} in Fig. 2(b)). The interpolated value from grid nodes of $T_{i,j}$ and $T_{i+1,j}$ is located grid size apart from the interface to prevent instability. More detail description of the basic concept can be found in Reference [20]. Yang and Udaykumar [17] used a similar concept but they used the nearest grid point (point $T_{i,j}$) instead. By keeping a certain distance from the interface, gradient term can be safely obtained without overshooting from excessive proximity of the phase boundary and the grid node. General process can be formulated as follows for effective implementation. Let evaporation temperature be T_f then:

$$s_{\pm x}=\frac{\phi_{i,j,k}\phi_{i\pm1,j}}{|\phi_{i,j,k}\phi_{i\pm1,j}|} \quad (3)$$

$$\lambda_{\pm x}=\left|\frac{\phi_{i\pm1,j}}{\phi_{i\pm1,j}-\phi_{i,j}}\right| \quad (4)$$

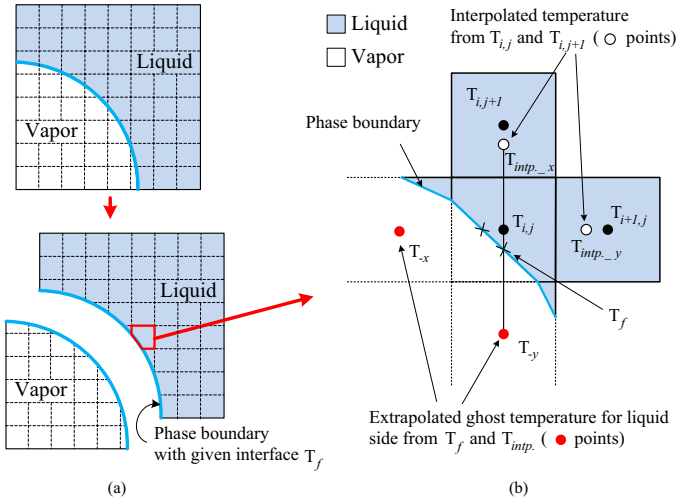

Fig. 2. Schematic diagram of the proposed sharp energy formulation. (a) Separation of the simulation domain into liquid and gas phases; (b) extrapolation of the ghost points for the liquid side.

$$T_{\pm x} = [(1+\lambda_{\pm x})T_f - \lambda_{\pm x}^2 T_{i\mp1,j} - \lambda_{\pm x}(1-\lambda_{\pm x})T_{i,j}]|\min(s_{\pm x},0)| + T_{i\pm1,j}|\max(s_{\pm x},0)| = (1+\lambda_{\pm x})|\min(s_{\pm x},0)|T_f - \lambda_{\pm x}^2|\min(s_{\pm x},0)|T_{i\mp1,j} + |\max(s_{\pm x},0)|T_{i\pm1,j} - \lambda_{\pm x}(1-\lambda_{\pm x})|\min(s_{\pm x},0)|T_{i,j} \quad (5)$$

Similar formulation can be applied to the y direction. The same procedure will be applied to the computation of the ghost point values for the gas phase.

2.3. Solution procedure

The basic process for solving Navier–Stokes equation can be found in References [20–24], and we will briefly summarize the hydraulic part and focus again on phase changing formulation. The single form of the governing equation for two phase flow will be described by following equations considering liquid–vapor phase change at the interface:

$$\nabla\cdot\mathbf{u} = \mathrm{M} \quad (6)$$

$$\rho\left(\frac{\partial\mathbf{u}}{\partial t} + \mathbf{u}\cdot\nabla\mathbf{u}\right) = -\nabla P + \rho\mathbf{g} + \nabla\cdot\mu\left(\nabla\mathbf{u} + \nabla\mathbf{u}^{\mathrm{T}}\right) + \mathbf{F} \quad (7)$$

$$\frac{\partial T}{\partial t} + \mathbf{u}\nabla T = \alpha\nabla^2 T \begin{cases} \alpha = \alpha_L & \text{for liquid} \\ \alpha = \alpha_G & \text{for vapor} \end{cases} \quad (8)$$

where u is the velocity, P is the pressure, and g is the gravitational acceleration. Hybrid form was used to describe the surface tension term F as follows:

$$\mathbf{F} = \sigma\kappa_H\nabla I \quad (9)$$

where σ is the surface tension coefficient assumed to be constant. Hybrid form of the interface curvature field, κ_H, can be calculated on Eulerian grid following the procedure described in References [23,24]. I is the Heaviside function that is computed directly from the Lagrangian interface. Functional distribution of I is also used to describe material properties of density and viscosity for the momentum equation through the entire simulation domain.

$$\rho = \rho_L + (\rho_G - \rho_L)I \quad (10)$$

$$\mu = \mu_L + (\mu_G - \mu_L)I \quad (11)$$

More detailed description of the solution procedure for the momentum equation can be found in References [20–24].

In the current paper, we will concentrate on formulation of the phase changing term in governing equations. M in Eq. (6) represents the mass source term at the interface, which describes phase change between liquid and gas. There exist several different formulations for the mass source at the phase interface as follows:

$$M = \frac{(\rho_G - \rho_L)}{\rho_L\rho_G}\int_A \dot{m}_f\delta(\mathbf{x}-\mathbf{x}_f)dA \quad \text{(CASE A)} \quad (12)$$

$$M = \frac{(\rho_G - \rho_L)}{\rho_f\rho}\int_A \dot{m}_f\delta(\mathbf{x}-\mathbf{x}_f)dA \quad \text{(CASE B)} \quad (13)$$

$$M = \frac{(\rho_G - \rho_L)}{\rho^2}\int_A \dot{m}_f\delta(\mathbf{x}-\mathbf{x}_f)dA \quad \text{(CASE C)} \quad (14)$$

Here, $\dot{m}_f$ is the mass flux and ρ_f is the density at the interface, respectively. Density field (ρ) is defined by Eq. (10). References [6,8,10,18,19] utilize the formulation of Eq. (12). Eq. (14) was used in Level Set based methods [5,7,9]. Eq. (13) was slightly modified, which was used in Reference [4]. Detailed derivation of each equation (12), (13), and (14) can be found in the related references.

The mass flux at the interface is computed using the following equation:

$$\dot{m}_f h_{fg} = -k_G\frac{\partial T}{\partial n}\Big)_G + k_L\frac{\partial T}{\partial n}\Big)_L \quad (15)$$

The gradient of temperature at each phase can be computed directly by probing technique of Udaykumar et al. [25]. Since our interface tracking method is based on Front Tracking, calculation of the temperature gradient is very straightforward given the normal and fixed temperature conditions at the interface.

Equations described from (12) to (14) show very similar forms except division of densities. Density at the interface can be assumed as averaged value between the gas and the liquid. We tested two different averages of arithmetic (ρ_{f_A}, Eq. (16)) and harmonic (ρ_{f_H}, Eq. (17)) for the inverse of the interface density (ρ_f) in Eq. (13).

$$\frac{1}{\rho_{f\_A}} = \frac{2}{\rho_G + \rho_L} \quad (16)$$

$$\frac{1}{\rho_{f\_H}} = \frac{1}{2}\left(\frac{1}{\rho_L} + \frac{1}{\rho_G}\right) \quad (17)$$

The Lagrangian elements of the interface are advected by integrating:

$$\frac{d\mathbf{x}_f}{dt} = \mathbf{u} + \frac{\dot{m}_f}{\rho_f}\mathbf{n} \quad (18)$$

with a second order Runge–Kutta method where the interface velocity, V, is interpolated from the Eulerian velocity. Here, density at the phase interface can also be approximated either with Eq. (16) or with Eq. (17). We will evaluate the accuracy of the formulations (Eqs. (12)–(14)) for the mass source term in the next section considering the different forms of the phase density (Eqs. 16 and 17).

3. Results and discussions

3.1. Comparison of phase change formulations

We presented three different formulations (Eqs. (12), (13), and (14)) of the mass generation term in Eq. (6) and two different averages of the phase density (Eqs. (16) and (17)). So there can be 6 possible combinations of the final formulation. We compared each formulation with the theoretical solution [19]. Growth bubble radius in a stagnant superheated liquid has analytical solution as:

$$R(t) = 2\beta\sqrt{\alpha_L t} \quad (19)$$

where α_L represents thermal diffusivity of the liquid. The growth constant β can be calculated by solving the following equation:

$$\frac{\rho_L c_L(T_\infty - T_{sat})}{\rho_G[h_{fg} + (c_L - c_G)(T_\infty - T_{sat})]} = 2\beta^2\int_0^1 \exp\left[-\beta^2\left\{(1-\zeta)^{-2} - 2\left(1-\frac{\rho_G}{\rho_L}\right)\zeta - 1\right\}\right]d\zeta \quad (20)$$

here, ρ and c are density and specific heat. h_{fg} stands for latent heat of vaporization. T_∞ represents superheated ambient temperature.

Axisymmetric geometry was used to simulate bubble growth in a stagnant liquid without gravity. We also solved half of the domain in the vertical direction, i.e. symmetric condition at the bottom. The other boundaries are set to open condition. Box size of 125 μm × 125 μm was used with the grid resolution of 256^2 to check

performance from the different mass source formulations. Our first intention was to find appropriate phase change formulation, so enough grid resolution, which guarantees mesh convergence, was utilized. Full grid convergence test will be followed in the next section. Material properties of water at 1 atm were used for the vapor and the liquid. Density, viscosity, heat capacity, and thermal conductivity of the vapor was 0.597 kg/m^3, 1.26×10^{-5} kg/m·s, 2030 J/kg·K, and 0.025 W/m·K, respectively, and those for the liquid were 958.4 kg/m^3, 2.8×10^{-4} kg/m·s, 4216 J/kg·K, and 0.679 W/m·K, respectively. Surface tension coefficient of 0.059 N/m was used and latent heat was set to 2.26×10^6 J/kg. Initially, radius of 50 μm was placed at the center of the simulation domain, which corresponds to the analytical solution at t = 0.016 ms. Initial temperature field was prescribed by analytical solution, and boundary condition of the temperature was also computed using analytical value at the given simulation time. The required input values and simulation settings are exactly same as in Sato and Niceno [19].

Time growth of the bubble radius was plotted in Fig. 3 with various options of the mass generation formulation. Six different test cases were simulated to check the accuracy of the phase change formulation. Analytical solution was also plotted on top of the simulation results. We denoted mass generation options as A, B, and C correspond to CASE A (Eq. (12)), CASE B (Eq. (13)), and CASE C (Eq. (14)), respectively. Average density at the interface was also denoted as ρ_{f_A} (arithmetic) and ρ_{f_H} (harmonic). As can be seen from the graph, CASE A with harmonic average generates correct radial growth of the bubble. CASE B and C show increased mass generation at given phase density due to division of low density of the vapor phase in the density field (ρ). With increased density ratio, arithmetic average has large value compared to harmonic average. So interface advection computed by Eq. (18) predicts much lower increment. Except CASE A with harmonic average for the phase density, the other formulations show large discrepancy from the theoretical value. We have to note that current formulation of the mass generation was included in the mass conservation equation using delta function in the frame work of Front Tracking method, and the mass flux was also evaluated directly on the interface. So the procedure is not exactly matching the one proposed by Level Set and VOF method [5,9,10,18,19]. Mass generation formulation of CASE A with harmonic phase density will be used for the entire test cases.

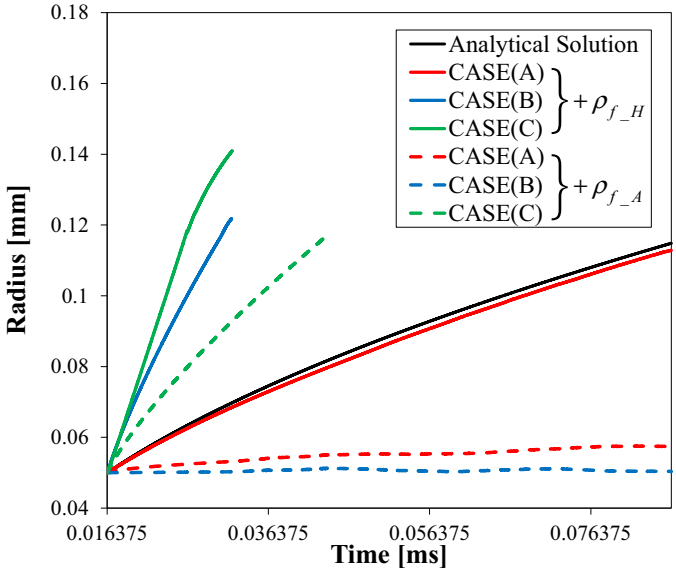

Fig. 3. Comparison of the various formulations for the mass source term with different density averages at the phase interface.

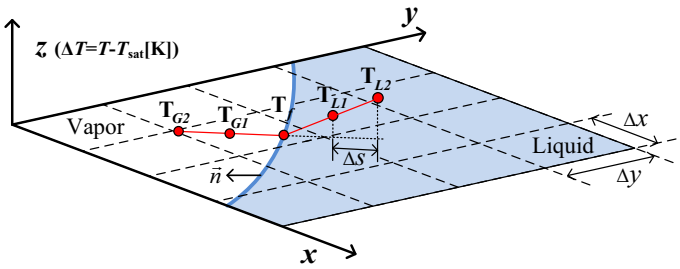

Fig. 4. Probing procedure for the evaluation of first and second order temperature gradients at the interface.

3.2. Optimized distance for probing technique

To obtain mass transfer rate at the interface (Eq. (15)), we used probing technique of Udaykumar et al. [25]. Fig. 4 shows a schematic diagram of the temperature probing. For example, first order temperature gradient at the gas region can be computed as follows:

$$\left.\frac{\partial T}{\partial n}\right)_G = \frac{T_{G1}-T_f}{\Delta s} \tag{21}$$

Here, T_{G1} is the interpolated temperature normal to the interface with distance Δs. We can select arbitrary distance for the probing temperature from the interface. Liquid side gradient can be calculated in similar fashion. For the tests in section 3.1, we used grid size as the probing distance. We can also utilize second order method for the temperature gradients in Eq. (15). In this case, probing needs to be performed on two different locations from the interface (points T_{G1} and T_{G2} in Fig. 4). Constant probing distance is used to acquire the temperature values. Thus, second order temperature gradient can be formulated as:

$$\left.\frac{\partial T}{\partial n}\right)_G = \frac{-T_{G2}+4T_{G1}-3T_f}{2\Delta s} \tag{22}$$

Here, T_{G2} is the interpolated temperature with twice the distance of T_{G1}.

Full grid convergence tests were performed with both first and second order gradients for the probing technique. The results were summarized in Fig. 5. L_2 norm defined as Eq. (23) was compared with different grid resolutions.

$$L_2 = \left[\frac{1}{N}\left(\sum_{i=1}^{N}|R_{cal}-R_{theory}|^2\right)\right]^{1/2} \tag{23}$$

Here, i represents discrete index and N is the total data points. R_{cal} is from the simulation and R_{theory} was computed value from theoretical Eq. (19).

For the first order method, the results show grid convergence with decreasing mesh size as can be seen from Fig. 5. We will denote probing distance as normalized distance from the interface to the probing point by mesh size. Probing distance of 0.75 shows promising convergence behavior up to a certain resolution, but at the highest resolution, the error is almost comparable to probing distance of one grid size. The other probing distance higher than grid size shows mostly 1st order convergence throughout the considered resolution range. Accuracy with probing distance of 0.5 is deteriorating quickly with increased grid resolution. On the other hand, the L_2 norm is not converging with increased resolution for the second order method. At lower resolution, error is decreasing with 1st order accuracy and shorter probing distance shows higher convergence rate. With increased resolution, error deteriorates significantly. This is because the second order method utilizing higher

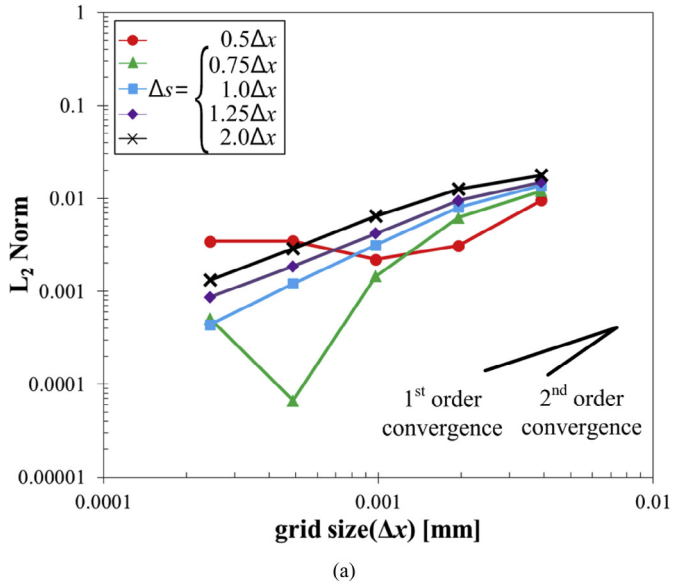

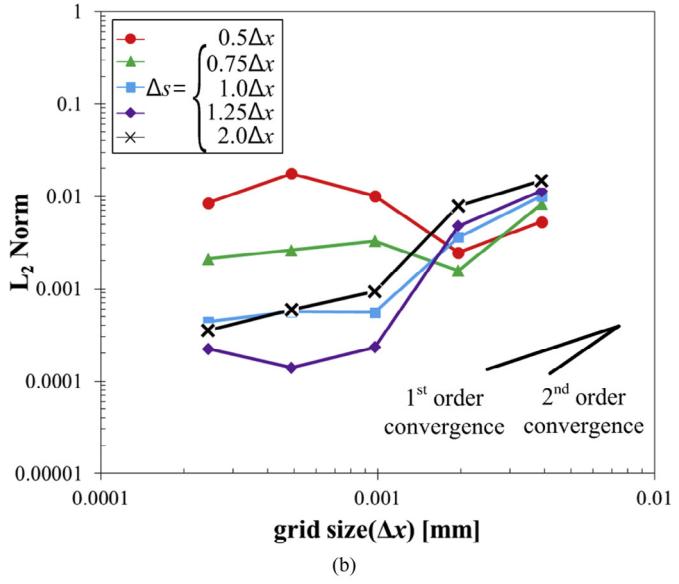

Fig. 5. Error analysis for the growth of a bubble in a stagnant liquid with zero gravity: (a) first order and (b) second order approximation of the temperature gradient at the interface. (For interpretation of the references to color in this figure legend, the reader is referred to the web version of this article.)

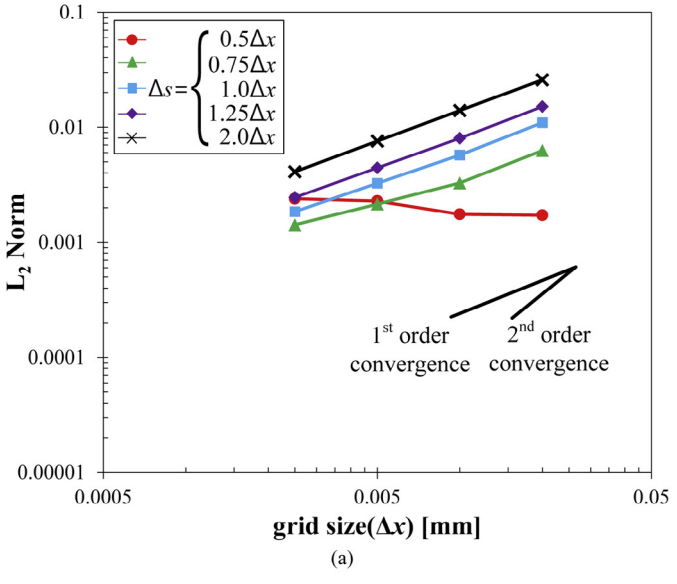

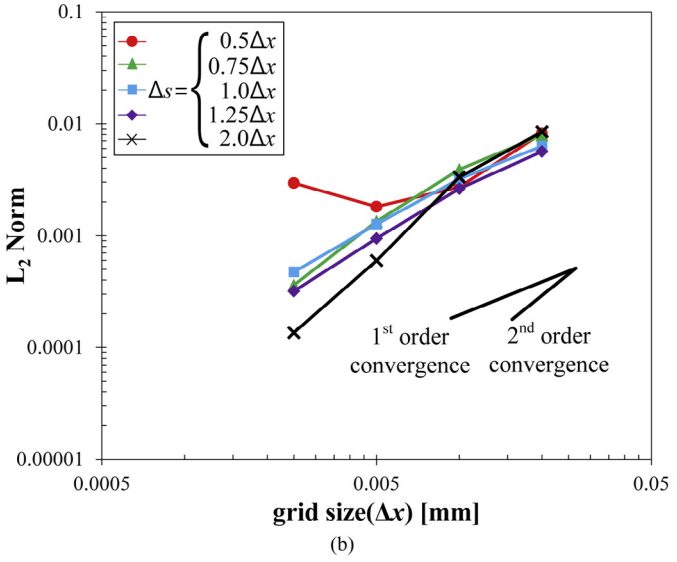

Fig. 6. Error analysis for the Stefan problem: (a) first order and (b) second order approximation of the temperature gradient at the interface.

order polynomial such as Eq. (22) is sensitive to data perturbation especially at increased resolution. Temperature distribution near the interface will experience slight perturbation by the mass generation from phase change.

To check the validity of above assumption, simple melting problem, i.e. Stefan problem, was performed [19,20]. Simulation geometry is very similar to the above except using planar surface instead of axisymmetric one. Constant thermal diffusivity was assigned for both phases. In this case, mass generation can be ignored from no density difference between liquid and solid. Analytical solution exists for 1-D problem in infinite domain with simple initial and boundary condition. Initially, zero temperature was set to the entire domain then the center of the domain maintains a fixed temperature throughout the simulation. More detailed description of the simulation settings can be found in Reference [20]. Again, L_2 norm from the Stefan problem was plotted in Fig. 6. As can be seen from the figure, both methods demonstrated converging behavior with increased resolution. The second order method showed higher convergence rate compared to the first order method. This supports that the mass generation from the interface is causing instabilities for the second order gradient approximation. One thing to note is that the accuracy deteriorates with decreased mesh size at the small probing distance. This behavior was already noticed with the bubble growth case above (Fig. 5(a) and (b)). With first order approximation of the temperature gradient, the error was increased at the highest resolution with the probing distance of 0.5. Similar behavior can also be found in second order method with the probing distances of 0.5 and 0.75.

We investigated these phenomena more in detail. Our sharp energy formulation interpolates temperature near the interface for the temperature gradients to compute the mass generation term of Eq. (15). As can be seen from Fig. 4, grid node for the temperature interpolation may not be located in the same phase. Since ghost values of each phase are not explicitly updated, referencing the temperature value outside the phase will decrease the solution accuracy.

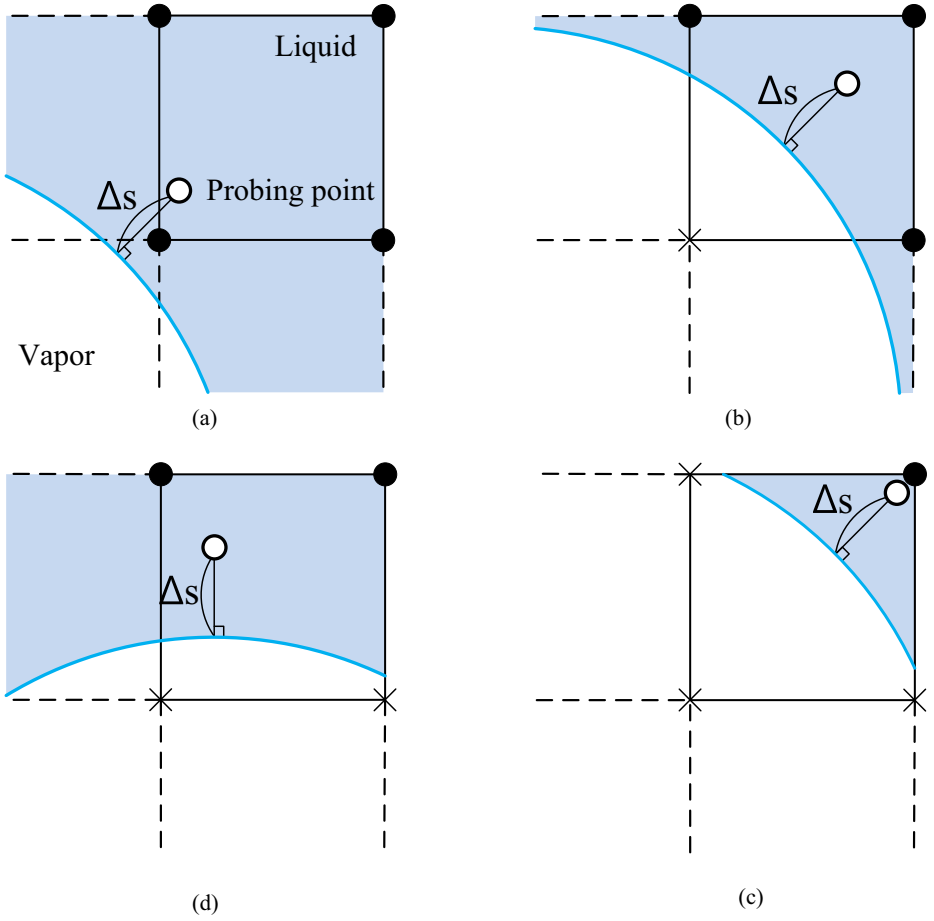

Fig. 7. Description of four different cases for possible temperature interpolation near the interface: (a) all four nodes, (b) three nodes, (c) two nodes, and (d) only one node in the same phase.

We can extrapolate ghost value at each time step using appropriate propagation equation similar to the work of Sato and Niceno [19] but this will cost significant computational time. We categorized four different cases of temperature interpolation for the probing by counting the number of nodes in the required phase (see Fig. 7). All node points for the interpolation can be in the same phase as in Fig. 7(a) (node #4). Depending on the interface location, three nodes (node #3), two nodes (node #2), and one node (node #1) can be positioned at the required phase. In Fig. 8, we draw probability for the node count of the four different cases with the bubble growth test. As can be seen from the graph, the case of only one node in the required phase is starting to happen at lower probing distance. At higher probing distance, most of the probing cells consist of four nodes in the required phase, but the accuracy of the computed gradient would be decreased. For proper interpolation of the temperature, at least three different points are necessary. This explains the proper convergence behavior with probing distance higher than grid size (i.e. 1.0Δx). At the probing distance of 0.75, majority (around 90%) of the interpolation would be performed more than two points in the required phase. Since we placed zero value for the ghost points outside the required phase and the phase interface temperature has been scaled to zero, the case of two node points could be working well with certain probing distance (see green line in Fig. 5(a) case of 0.75Δx) up to a certain grid resolution. This could explain the sudden decrease of L_2 error norm in Fig. 5(a). With consideration of the limited computational resources, grid resolution cannot be increased high enough. Thus, it could be practical to use probing distance of 0.75 for proper solution.

The time dependent growth of the bubble radius is described in Fig. 9(a). The probing distance of 0.75 was selected as optimal number in considered grid resolution. With increased resolution, growth radius is matching very well with the theoretical solution. We also plotted

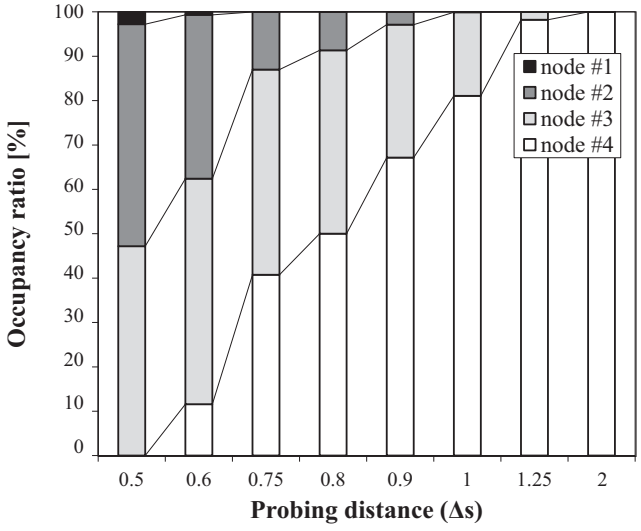

Fig. 8. Probability distribution of the inner node counts with different probing distances during the bubble growth test.

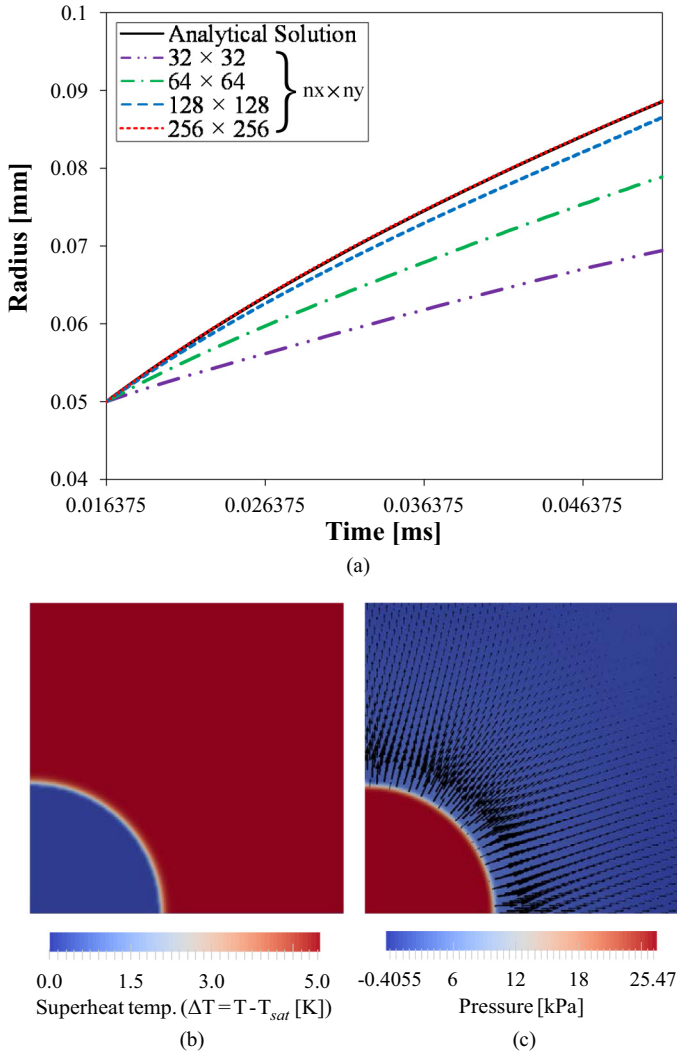

Fig. 9. Results from the bubble growth test: (a) the time dependent growth of the bubble radius with different grid resolutions; (b) temperature and (c) pressure distribution with velocity vector at the highest resolution.

temperature distribution as well as pressure distribution with vector field in Fig. 9(b) and (c), respectively. We can see the symmetrical thin thermal layer (transition zone of the temperature) at the phase interface with outward velocity describing mass generation. Pressure jump across the interface was correctly captured and the velocity profile is well defined without any parasitic current.

3.3. Simulation of a rising bubble with phase change

Final benchmarking test was performed on a bubble rising with phase change. Bubble rise behavior has been studied widely for its own physical importance [26] and also frequently used as benchmarking solution for numerical schemes related to hydrodynamic part of the formulation [27]. Considering the long travel distance of a rising bubble, we utilized moving domain for the simulation geometry. Schematic of the simulation geometry is described in Fig. 10. Symmetric condition is used for the left side boundary, and free slip condition in y direction was applied at the right side. Open condition was used at the top and bottom boundaries. Initially, a spherical bubble was placed at the center of the simulation domain. A coordinate transformation of the velocity, pressure, temperature, and interface location was implemented to maintain the bubble location inside the simulation domain [28].

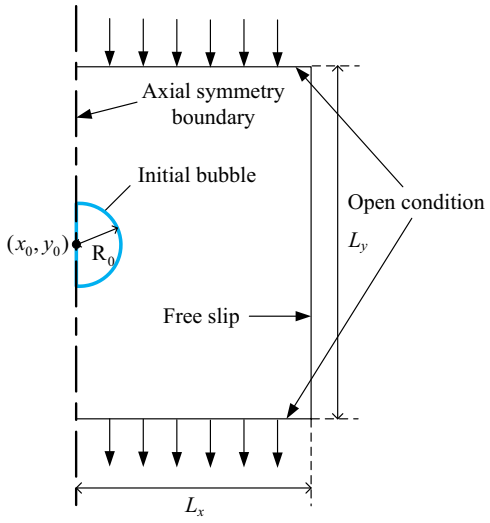

Fig. 10. Simulation geometry for the bubble rising test with moving boundary.

At first, non-evaporating bubble rising in a stagnant liquid was carried out to validate the accuracy of the moving reference frame. The terminal velocity of a rising bubble depends on non-dimensional parameters of Re ($=\rho_L g^{0.5} R^{1.5}/\mu_L$) and We ($=\rho_L g R^2/\sigma$) numbers. Case (b) of table 1 of Son [29] was selected for comparison. A sphere with unit radius was placed in 6×12 ($=L_x \times L_y$) simulation box. Reynolds number of 8.66 and Weber number of 1.26 were used with density ratio as 1000 and viscosity ratio as 55.5, respectively. The rising velocity for three different resolutions of 32×64, 64×128, and 128×256 was plotted in Fig. 11. With increased resolution, the rising velocity is converging to constant value of 1.12 close to 1.16 from the work of Son [29]. The result shows that the moving domain is working properly.

Next, we have simulated a bubble rise with phase change, which is identical to the simulation performed by Sato and Niceno [19]. Exactly the same simulation settings of Sato and Niceno [19] were used in this study except the moving domain. With initial sensitivity tests for the domain size, we found out that the box size of 3×4.5 mm ($=L_x \times L_y$ in Fig. 10) was sufficient for the converged solution. Initially, a vapor bubble with radius of 0.21 mm is located

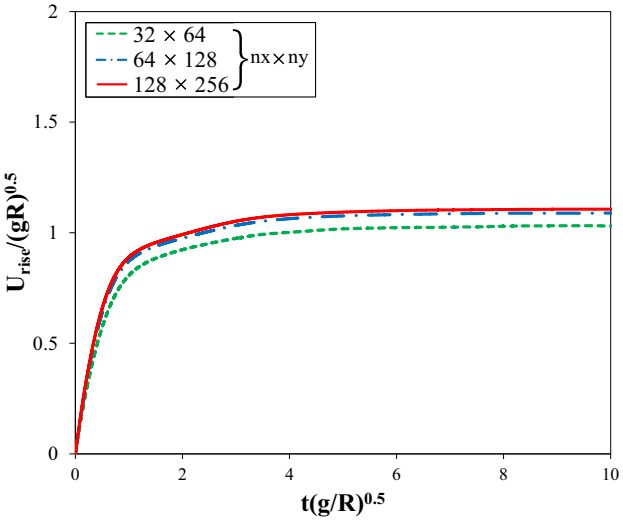

Fig. 11. Rising velocity from a non-evaporating bubble with different grid resolutions for the validation of the moving boundary.

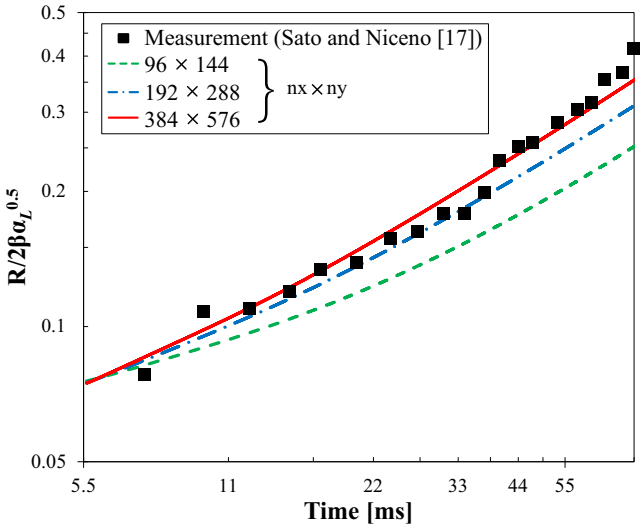

Fig. 12. Comparison of the radius of the rising bubble with experimental data.

at the center of the simulation domain. The initial temperature distribution was computed using analytical solution with zero gravity at the time of 0.0056 s. Ethanol was selected as a working fluid. Density, viscosity, heat capacity, and thermal conductivity of the vapor were 1.435 kg/m^3, 1.04×10^{-5} kg/m·s, 1830 J/kg·K, and 0.02 W/m·K, respectively, and those for the liquid were 757 kg/m^3, 4.29×10^{-4} kg/m·s, 3000 J/kg·K, and 0.154 W/m·K, respectively. Surface tension coefficient of 0.018 N/m was used, and latent heat was set to 9.63×10^6 J/kg. The liquid superheat was set to 3.1 K as in Reference [19]. The radius of the rising bubble was compared with experimental result at Fig. 12. Three different resolutions of 96×144, 192×288, and 384×576 were tested for grid convergence. In our simulation, grid resolution of 384×576 matches the fine grid and 192×288 matches the coarse grid in the work of Sato and Niceno [19]. The growth radius shows converging behavior with increased resolution and the growth rate at the highest resolution is in good agreement with experimental data.

The evolution of the temperature distribution measured from saturation value at different time step was shown in Fig. 13. Velocity vector for the last frame was also included in the figure. As the bubble rises, initial spherical shape is changed to ellipsoid, and winding vortex at the side of the bubble can be clearly seen. In Fig. 14, we plotted the rising velocity of the growing bubble with phase change along with those from non-evaporating bubbles. Initial and final radius from Fig. 13 was selected as comparison for the rising velocity of the non-evaporating bubbles. The rising velocity of the evaporating bubble is initially increasing to the maximum value then decreasing, similar to the result from Sato and Niceno [19]. The rising velocity of the small bubble without phase change quickly converges to a constant value. On the other hand, the rise velocity of the large non-evaporating bubble is starting to oscillate after initial increase. Since the Reynolds number for the large bubble is around 230, the rising bubble will be very unstable as found in Reference [30]. Due to the gradual change of the radius for the evaporating bubble, the rising velocity is in the middle without oscillation.

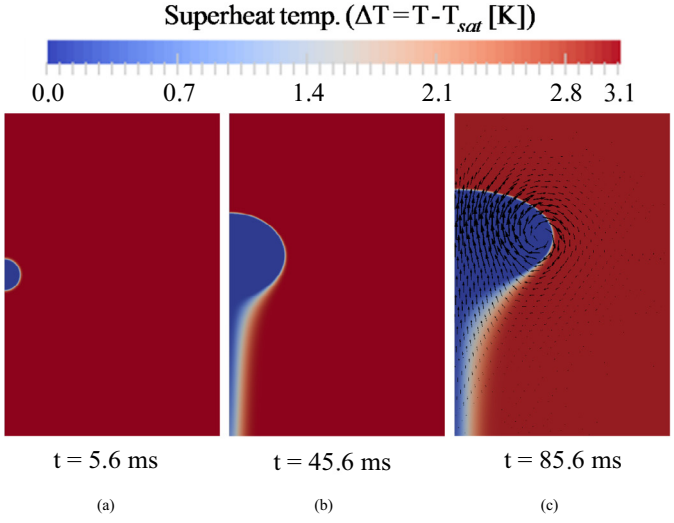

Fig. 13. Interface evolution of the rising bubble with phase change at the highest resolution. Velocity plot for the final frame was also included.

4. Conclusion

Phase changing phenomenon is a very important process utilized in various engineering applications. Due to small space and time scale related to phase change, a numerical tool can be ideal for the analysis of underlying physical behavior that can be controlled for higher system efficiency. Multiphase flow dynamics has been widely treated with numerical techniques and has shown remarkable success. Most two-phase numerical formulations have been focused on the hydraulic part of the simulation. Direct simulation of the phase change for two-phase flow is relatively new and is gathering attention for possible application for boiling process. Since phase changing formulation requires not only precise tracking ability for the moving interface but also correct computation of mass generation at the phase changing interface, it puts additional difficulties on the development of a numerical technique for multiphase dynamics.

The main goal of the current study was to increase the accuracy and implementation efficiency of sharp energy method for phase change problem in context of Front Tracking method. Key findings can be summarized as follows:

(1) Existing sharp energy method utilizes given temperature value at the interface and the nearest grid point. With close proximity of the interface to the grid, this formulation can generate excessive gradient that can lead to solution instability. We proposed a modified version of sharp energy method by positioning the interpolating inner point for temperature gradient with specific grid size from the interface, which can alleviate the solution instability.
(2) General discretization operator for the diffusion term readily expandable to three dimensions has been described for efficient implementation of the proposed method.
(3) There exist several different formulations for computing mass transfer rate during phase change in Front Tracking method. Three different formulations for the mass source term with two different phase density averages were compared with theoretical solution of bubble growth in a stagnant superheated liquid. Formulation using density values at each phase with harmonic average at phase interface showed most accurate result compared to analytic solution.
(4) To calculate mass flux at the interface, probing technique of Udaykumar et al. [25] was utilized. We tested various probing distance values on solution accuracy. Specific probing distance (0.75 of the grid size) showed optimal convergence rate in considered grid resolution for bubble growth simulation.
(5) Full convergence test in bubble growth simulation showed that first order approximation of the temperature gradients by probing technique performs better compared to second

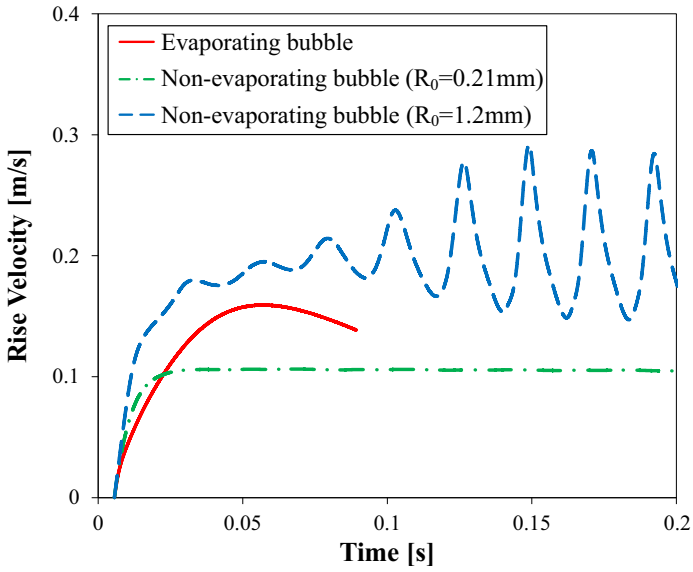

Fig. 14. Rising velocity of the bubble with phase change in comparison with the rise velocity of non-evaporating bubble started from its minimum and maximum radii.

order method since second order method is sensitive to the perturbation generated from the mass transfer at the interface.

(6) To check the validity of current formulation with dynamic situation, bubble rise with phase change was also compared with experimental data and showed good agreement.

Acknowledgements

This research was supported by the Basic Science Research Program through the National Research Foundation of Korea (NRF) funded by the Ministry of Science, ICT and Future Planning (NRF-2014R1A2A1A11051346)

Nomenclature

T	Temperature [K]
P	Pressure [Pa]
u	Velocity [m/s]
ρ	Density [kg/m^3]
k	Thermal conductivity [W/m·K]
c	Specific heat [J/kg·K]
μ	Viscosity [kg/m·s]
α	Thermal diffusivity [m^2/s]
h_{fg}	Latent heat of vaporization [J/kg]
σ	Surface tension coefficient
$\dot{m}$	Mass flux [kg/m^2·s]
Re	Reynolds number
We	Weber number
ϕ	Distance function
g	Gravitational acceleration [m/s^2]
κ	Mean curvature field
I	Heaviside function
β	Growth constant

Subscripts

L	Liquid phase
G	Gas phase
f	Interface
A	Arithmetic average
H	Harmonic average

References

[1] G. Tryggvason, R. Scardovelli, S. Zaleski, Direct Numerical Simulations of Gas-Liquid Multiphase Flows, Cambridge University Press, Cambridge, England, 2011.
[2] C.W. Hirt, B.D. Nichols, Volume of fluid (VOF) method for the dynamics of free boundaries, J. Comp. Phys. 39 (1981) 201–225.
[3] S. Osher, R.P. Fedkiw, Level set methods: an overview and some recent results, J. Comp. Phys. 169 (2001) 463–502.
[4] D. Juric, G. Tryggvason, Computations of boiling flows, Int. J. Multiphase Flow 24 (1998) 387–410.
[5] G. Son, V.K. Dhir, N. Ramanujapu, Dynamics and heat transfer associated with a single bubble during nucleate boiling on a horizontal surface, J. Heat Transfer 121 (1999) 623–631.
[6] A. Esmaeeli, G. Tryggvason, Computations of film boiling. Part I: numerical method, Int. J. Heat Mass Transf. 47 (2004) 5451–5461.
[7] X. Luo, M. Ni, A. Ying, M.A. Abdou, Numerical modelling for multiphase incompressible flow with phase change, Numer Heat Transf Part B 48 (2005) 425–444.
[8] A. Esmaeeli, G. Tryggvason, A front tracking method for computations of boiling in complex geometries, Int. J. Multiphase Flow 30 (7) (2004) 1037–1050.
[9] G. Son, V.K. Dhir, A level set method for analysis of film boiling on an immersed solid surface, Numer Heat Transf Part B 52 (2007) 153–177.
[10] M.H. Yuan, Y.H. Yang, T.S. Li, Z.H. Hu, Numerical simulation of film boiling on a sphere with a volume of fluid interface tracking method, Int. J. Heat Mass Transf. 51 (2008) 1646–1657.
[11] L. Zhang, Z. Li, H. Li, J. Zhao, Influence of heater thermal capacity on bubble dynamics and heat transfer in nucleate boiling, Appl. Therm. Eng. 88 (2015) 118–126.
[12] H.W. Jia, P. Zhang, X. Fu, S.C. Jiang, A numerical investigation of nucleate boiling at a constant surface temperature, Appl. Therm. Eng. 88 (2015) 248–257.
[13] R.P. Fedkiw, T. Aslam, B. Merriman, S. Osher, A non-oscillatory Eulerian approach to interfaces in multimaterial flows (the ghost fluid method), J. Comp. Phys. 152 (1999) 457–492.
[14] M. Sussman, K.M. Smith, M.Y. Hussaini, M. Ohta, R. Zhi-Wei, A sharp interface method for incompressible two-phase flows, J. Comp. Phys. 221 (2007) 469–505.
[15] H. Terashima, G. Tryggvason, A front-tracking/ghost-fluid method for fluid interfaces in compressible flows, J. Comp. Phys. (2009) 4012–4037.
[16] M. Kaneda, T. Haruna, K. Suga, Ghost-fluid-based boundary treatment in Lattice Boltzmann method and its extension to advancing boundary, Appl. Therm. Eng. 71 (2006) 126–134.
[17] Y. Yang, H.S. Udaykumar, Sharp interface Cartesian grid method III: solidification of pure materials and binary solutions, J. Comp. Phys. 210 (2005) 55–74.
[18] F. Gibou, L. Chen, D. Nguyen, S. Banerjee, A level set based sharp interface method for the multiphase incompressible Navier-Stokes equations with phase change, J. Comp. Phys. 222 (2007) 536–555.
[19] Y. Sato, B. Niceno, A sharp-interface phase change model for a mass-conservative interface tracking method, J. Comp. Phys. 249 (2013) 127–161.
[20] S. Shin, S.I. Abdel-Khalik, Numerical modelling of evaporating thin liquid film instability on a heated cylindrical rod with parallel and cross vapor flow, Nucl. Sci. Eng. 156 (2007) 1–16.

[21] S. Shin, D. Juric, Modeling three-dimensional multiphase flow using a level contour reconstruction method for front tracking without connectivity, J. Comp. Phys. 180 (2002) 427–470.
[22] S. Shin, D. Juric, High order level contour reconstruction method, J. Mech. Sci. Technol. 21 (2) (2007) 311–326.
[23] S. Shin, S.I. Abdel-Khalik, V. Daru, D. Juric, Accurate representation of surface tension using the level contour reconstruction method, J. Comp. Phys. 203 (2005) 493–516.
[24] S. Shin, D. Juric, A hybrid interface method for three-dimensional multiphase flows based on front-tracking and level set techniques, Int. J. Num. Meth. Fluids 60 (2009) 753–778.
[25] H.S. Udaykumar, R. Mittal, W. Shyy, Computation of solid-liquid phase fronts in the sharp interface limit on fixed grids, J. Comp. Phys. 153 (1999) 535–574.
[26] M.V.S. Annaland, N.G. Deen, J.A.M. Kuipers, Numerical simulation of gas bubbles behaviour using a three-dimensional volume of fluid method, Chem. Eng. Sci. 60 (2005) 2999–3011.
[27] T. Bonometti, J. Magnaudet, An interface-capturing method for incompressible two-phase flows. Validation and application to bubble dynamics, Int. J. Multiphase Flow 33 (2007) 109–133.
[28] M. Hase, B. Weigand, Transient heat transfer of deforming droplets at high Reynolds numbers, Int. J. Num. Meth. Heat Fluid Flow 14 (1) (2004) 85–97.
[29] G. Son, A numerical method for bubble motion with phase change, Numer Heat Transf Part B 39 (2001) 209–523.
[30] P.C. Duineveld, The rise velocity and shape of bubble in pure water at high Reynolds number, J. Fluid Mech. 292 (1995) 325–332.